

Robust scaling of strength and elastic constants and universal cooperativity in disordered colloidal micropillars

Daniel J. Strickland^a, Yun-Ru Huang^b, Daeyeon Lee^{b,1}, and Daniel S. Gianola^{a,1}

Departments of aMaterials Science and Engineering and bChemical and Biomolecular Engineering, University of Pennsylvania, Philadelphia, PA 19104

Edited by John W. Hutchinson, Harvard University, Cambridge, MA, and approved November 11, 2014 (received for review July 24, 2014)

We study the uniaxial compressive behavior of disordered colloidal free-standing micropillars composed of a bidisperse mixture of 3- and 6-µm polystyrene particles. Mechanical annealing of confined pillars enables variation of the packing fraction across the phase space of colloidal glasses. The measured normalized strengths and elastic moduli of the annealed freestanding micropillars span almost three orders of magnitude despite similar plastic morphology governed by shear banding. We measure a robust correlation between ultimate strengths and elastic constants that is invariant to relative humidity, implying a critical strain of ~0.01 that is strikingly similar to that observed in metallic glasses (MGs) [Johnson WL, Samwer K (2005) Phys Rev Lett 95:195501] and suggestive of a universal mode of cooperative plastic deformation. We estimate the characteristic strain of the underlying cooperative plastic event by considering the energy necessary to create an Eshelby-like ellipsoidal inclusion in an elastic matrix. We find that the characteristic strain is similar to that found in experiments and simulations of other disordered solids with distinct bonding and particle sizes, suggesting a universal criterion for the elastic to plastic transition in glassy materials with the capacity for finite plastic flow.

plasticity in disordered solids | shear transformation | cooperative deformation | Eshelby inclusion | colloidal glasses

n an ideal, defect-free system, the relationship between a material's elastic constants and yield strength is indicative of the underlying plastic event that generates macroscopic yielding. For the case of a crystalline solid, Frenkel predicted the ideal yield stress by estimating the energy necessary to cooperatively shear pristine crystallographic planes. The result estimates that the ideal shear strength, $\tau_{y,ideal}$, scales linearly with the shear modulus, μ , as $\tau_{y,ideal} = \mu/2\pi$ (1). This simple, yet striking, prediction implies a singular critical shear strain for yielding, irrespective of the material. Experimental strengths of crystalline metals, however, are found to fall orders of magnitude short of Frenkel's ideal strength, suggestive of plasticity generated by mechanisms other than cooperative slip. In real bulk crystals, microstructural defects, such as dislocations, grain boundaries, and surfaces, become plastically active at stresses well below $\tau_{v,ideal}$, implying a transition to a far less cooperative plastic deformation mechanism. Controlling the character and number density of these defects mediates the strength of crystals; for instance, the Hall-Petch relationship for polycrystals (2, 3) states that $\tau_v \sim d^{-1/2}$, where τ_v is the yield strength and d is the grain size (thus controlling the fraction of planar defects), and Taylor strengthening (4) predicts $\tau_v \sim \rho^{1/2}$, where ρ is the dislocation density. This ability to tailor material strength is a reflection of the large catalog of plastic events found in crystals and the associated broad range of energies necessary for their operation. In such defected crystals, the highly cooperative shear mechanism that defines the intrinsic ideal strength is superseded by mechanisms that require the motion of only a few atoms (e.g., dislocation glide or climb), rather than the coordinated motion of many atoms.

Metallic glasses (MGs)—amorphous alloys—on the other hand, exhibit a surprisingly robust relationship between yield strength and elastic constants despite their atomic heterogeneity and absence of long-range order. Various MG alloys have been synthe sized with shear moduli that range from 10 to 80 GPa (5). Remarkably, an approximately universal critical shear strain limit of $\gamma_{\nu} \approx 0.02$, where $\gamma_{\nu} = \tau_{\nu}/\mu$, has been measured (6) and directly demonstrated via atomistic simulations of MGs (7). Whereas structural modifications of the MGs through processes such as thermal treatment (8), severe plastic deformation (9), and ion-beam irradiation (10, 11) have been shown to alter the strength and ductility of MG alloys, the extent of strength variation is far below that of crystalline metals, which is suggestive of a single fundamental plastic event unique to MGs. Furthermore, the characteristic failure mode observed in MGs—"shear banding," in which plastic strain is localized in thin bands of the material—is also found in amorphous solids composed of nanoparticles, colloids, and grains (12-14). The fact that a common failure mode is observed in amorphous solids with very different characteristic length scales and interparticle interactions has led to the proposal that the fundamental plastic event found in MGs may in fact be universal to all amorphous solids. Indeed, direct visualizations of sheared 3D colloidal systems suggest cooperative shearing of collections of particles (13, 15, 16), although the link between these inelastic building blocks and macroscopic yielding is still not clear.

In this article, we report on free-standing amorphous colloidal micropillars with compressive strengths that also exhibit a robust correlation with elastic constants and thus a universal elastic

Significance

The mechanical response of glassy materials is important in numerous technological and natural processes, yet the link between the embryonic stages of plastic deformation and macroscopic mechanical failure remains elusive. The incipient inelastic rearrangements are believed to be highly cooperative and characterized by a scaling of yield strength and elastic constants. Whether this behavior transcends the nature of bonding is still an open question. Here, we show that disordered colloidal micropillars spanning the spectrum of glassy packing also demonstrate a robust scaling of elastic and plastic properties. Our measured relationship and deduced cooperative rearrangement strains bear striking resemblance to other glassy systems with disparate bonding, implying a universal building block for macroscopic flow.

Author contributions: D.J.S., D.L., and D.S.G. designed research; D.J.S. and Y.-R.H. performed research; D.J.S. and D.S.G. analyzed data; and D.J.S., D.L., and D.S.G. wrote

The authors declare no conflict of interest.

This article is a PNAS Direct Submission.

¹To whom correspondence may be addressed. Email: gianola@seas.upenn.edu or daeyeon@ seas.upenn.edu.

This article contains supporting information online at www.pnas.org/lookup/suppl/doi:10. 1073/pnas.1413900111/-/DCSupplemental

limit. By varying the packing fraction, ϕ , we are able to vary the maximum transmitted force, equivalent to strength, and the elastic constants over almost three orders of magnitude. We reconcile the robustness of the measured relationship by considering the energetics of the fundamental plastic event at criticality that is believed to underlie yielding in amorphous solids. This approach is based on the cooperative rearrangement first proposed by Argon following observations of sheared amorphous bubble rafts (17). The idea has since been extended in several models, including the cooperative shear model (CSM) of Johnson and Samwer (6, 18) and the shear transformation zone (STZ) theory of Falk and Langer (19, 20). Our analysis results in an estimation of the characteristic transformation strain of a cooperative rearrangement with a magnitude that bears striking resemblance to that estimated in MGs, supporting the notion of a characteristic cooperative mechanism for plasticity in amorphous solids.

We previously reported on a synthesis route for producing freestanding colloidal micropillars with cohesive particle-particle interactions (21). Briefly, capillaries are filled with colloidal suspensions, subsequently dried, and carefully extruded to produce free-standing specimens for uniaxial mechanical testing. The pillars relevant to the current work are 580 µm in diameter and composed of a bidisperse mixture of 3.00- and 6.15-µm-diameter polystyrene (PS) spheres. The mixture is prepared with a volume ratio $V_L/V_S \approx 1.0$, where V_L and V_S are the total volumes of the 6.15- and 3.00-µm spheres, respectively. The bidisperse mixture is chosen to suppress crystallization; optical and electron microscopies are used to confirm amorphous packing.

We developed a novel mechanical annealing procedure to alter the packing fraction ϕ —and consequently the mechanical response—which is described as follows. After allowing the suspension of colloidal particles to dry within the capillary tube, two steel wires with diameters slightly smaller than the capillary diameter are inserted into both ends of the tube, rendering the packing fully confined (Fig. 1A). A piezoelectric actuator is brought into contact with one of the wires and the opposite wire is coupled to a force transducer, enabling measurement of the axial force. Sinusoidal displacements (f = 0.5 - 5 Hz, $A = 0.60 - 3.60 \mu m$) are produced by the actuator, which remains in contact with the wire. The displacement periodically loads and unloads the pillar about the mean confining force ($F_{conf} \sim 0.1 - 10 \text{ N}$), resulting in a gradual densification of the pillar and an increase in ϕ . After mechanically annealing the pillar from one side, the capillary tube orientation is reversed, and the process is repeated from the other side to promote uniform compaction. Varying the confining force in addition to the amplitude, frequency, and number of displacement cycles allows for some control of compaction. Following annealing, the average packing fraction of the confined micropillar, $\langle \phi \rangle$, is determined by measuring the diameter, D, length, L, and mass, m_{filled} , using high-resolution optical microscopy and microbalance measurements, respectively. On completion of mechanical testing, the mass of the empty capillary tube, m_{empty} , is measured. Using the density of PS, ρ_{PS} , the packing fraction is determined as

$$\langle \phi \rangle = V_{solid}/V_{bulk} = \frac{\left(m_{filled} - m_{empty}\right)/\rho_{PS}}{\pi D^2 L/4}.$$

Our mechanical annealing procedure produced pillars with $0.528 \le \langle \phi \rangle \le 0.684$. For our mixture of particles, the random close packing limit (RCP) is predicted to be $\phi = 0.678$ (22). The lower bound, random loose packing (RLP), for a bidisperse mixture of frictional, cohesive particles is not known, but rheology measurements on a bidisperse mixture of hard spheres with similar diameter $\left(\frac{D_L}{D_S}\right)$ and total volume $\left(\frac{V_L}{V_S}\right)$ ratios show a fluidity limit, marked by a large increase in viscosity, at $\phi \approx 0.53$ (23). Thus, our pillars span the full spectrum of glass packing.

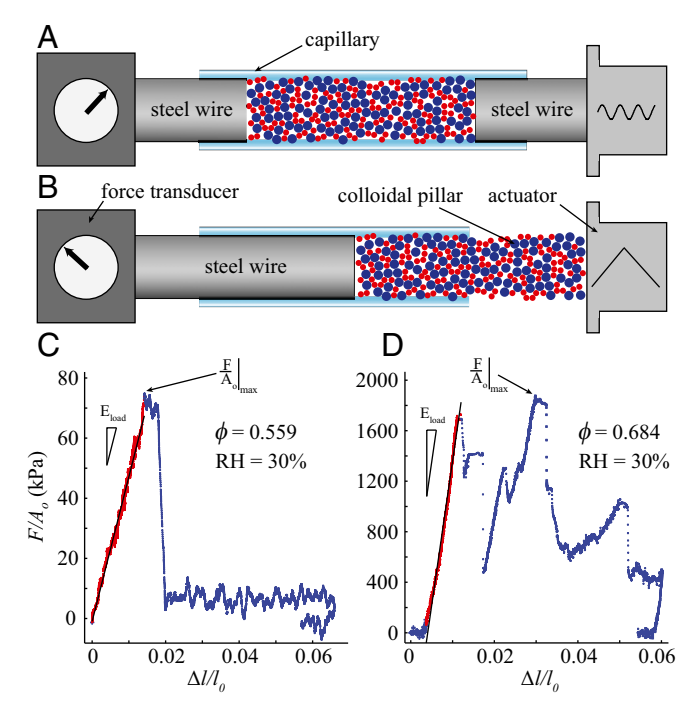


Fig. 1. (A) The mechanical annealing setup. The colloidal pillar is confined within a capillary by two steel wires between the actuator and the force transducer, and a sinusoidal displacement is generated by the actuator, leading to compaction of the pillar. (B) The uniaxial compression setup. Extruding the pillar results in a freestanding sample that is compressed in situ in a confocal microscope. (C) Mechanical response of a lightly annealed pillar with $\langle \phi \rangle$ = 0.559 compressed at 30% RH. The measured effective elastic modulus is E_{load} = 4.81 MPa and σ_{max} = 74.8 kPa. (D) Mechanical response of a highly annealed pillar with $\langle \phi \rangle = 0.684$ compressed at 30% RH, resulting in E_{load} = 229 MPa and σ_{max} = 1,880 kPa.

Following our annealing steps, the micropillars were prepared for uniaxial compression. The micropillars are made free standing by extruding a desired length from the capillary using a precision drive screw (Fig. 1B). As the pillars are oriented with their major axes perpendicular to the force of gravity, the stability of our free-standing micropillars suggests strong cohesive particleparticle interactions. Between one and four free-standing specimens are obtained from each capillary, and thus fluctuations in $\langle \phi \rangle$ from specimen to specimen are not quantified. We opted for the pillar geometry owing to both a nominally simple (uniaxial) stress state and for facile comparison with previous work on MGs (24-26). Our experimental setup also contains an environmental chamber, enabling control of the relative humidity (RH) during testing. Our previous work has shown that RH can alter the stiffness of a single pillar, which we attribute to variations in the amount of water contained within the pillar structure, affecting the number and connectivity of capillary bridges that form between particles (and thus the cohesive interactions) (21). Reflectance confocal micrographs acquired during compression are used to digitally determine the displacement of the punch and the base of the pillar and therefore allow axial strain within the pillar to be calculated. For more details on the experimental setup, refer to ref. 21.

Mechanical responses for specimens with $\langle \phi \rangle = 0.559$ and $\langle \phi \rangle =$ 0.684 are shown in Fig. 1 C and D. Both specimens exhibit an initial loading regime where the transmitted force, F, increases linearly with $\Delta l/l_o$ (Δl and l_o are the change in length and undeformed length of the pillar, respectively). For the $\langle \phi \rangle = 0.559$ specimen, significant structural evolution is observed in the micrographs for $\Delta l/l_o > \Delta l/l_o|_{F_{max}}$, and the subsequent load drop

correlates with the development of a system-spanning shear band. Further displacement shears the pillar along the band until final fracture. The $\langle \phi \rangle = 0.684$ specimen exhibits a series of elastic loadings and load drops that correspond with the formation of multiple shear bands. A plastic morphology characterized by one or more shear bands, typically emanating from the punch, is consistently observed, irrespective of $\langle \phi \rangle$ (Fig. S1). We define the ultimate compressive strength of the micropillars as the maximum normalized force, $F_{max}/A_o \equiv \sigma_{max}$ (A_o) is the cross-sectional area of the undeformed pillar), sustained by a pillar during a compression cycle. We also define an effective elastic modulus on loading, E_{load} , based on a linear fit to F/A_o vs. $\Delta l/l_o$ between initial loading and the first yielding event. Previously, we measured the mechanical dissipation in a dense micropillar at different RHs (21). Briefly, we found that at RHs up to ~30%, ~80% of the work done on loading was recovered on unloading for small total strains ($\Delta l/l_o \sim 0.003$). Increasing RH beyond 30% reduced the amount of energy recovered on unloading. Neglecting dissipation results in an underestimation of the elastic component of stiffness (see analysis in SI Text and Figs. S2 and S3); the consequences of underestimating the true elastic modulus will be discussed later.

The measured ultimate strengths and effective elastic moduli for 27 micropillar specimens are shown in Fig 2 A and B. Both F_{max}/A_o and E_{load} are found to vary by more than 2.5 orders of magnitude over the range of $\langle \phi \rangle$ studied, corresponding to

relatively loose and dense packings in the limit of low and high $\langle \phi \rangle$, respectively. We contend that σ_{max} is the best measure of the intrinsic strength of the pillar because plastic activity localized near the punch, which occurs at lower levels of applied stress, is likely a result of surface roughness and not representative of the of the bulk structure of the micropillar. Surprisingly, σ_{max} and E_{load} appear to be relatively insensitive to RH in the range covered in these experiments.

Our measurements demonstrate a strong correlation between σ_{max} and E_{load} of individual disordered micropillars (Fig. 2C), with a slope of 0.009 ± 0.0009 that is invariant to $\langle \phi \rangle$ and RH (shown by coloring and shape of markers, respectively, in Fig. 2C). The robust relationship between σ_{max} and E_{load} is suggestive of a unique and cooperative plastic event that establishes the maximum strain the micropillars can withstand before macroscopically failing. The insensitivity of this universal scaling to RH also suggests that the details of interparticle interactions do not influence the critical strain, which implies a plasticity mechanism that is universal to disordered solids with the capacity for finite plastic flow. This notion is further bolstered by the remarkable similarity of our measured scaling to that compiled from compressive behavior of MGs by Johnson and Samwer (6) as shown in Fig. 2C. We further note that such scaling between strength and elastic constants has been reported in atomistic simulations of nanocrystalline alloys (27), which in the limit of diminishingly small grain sizes have been shown to exhibit cooperative

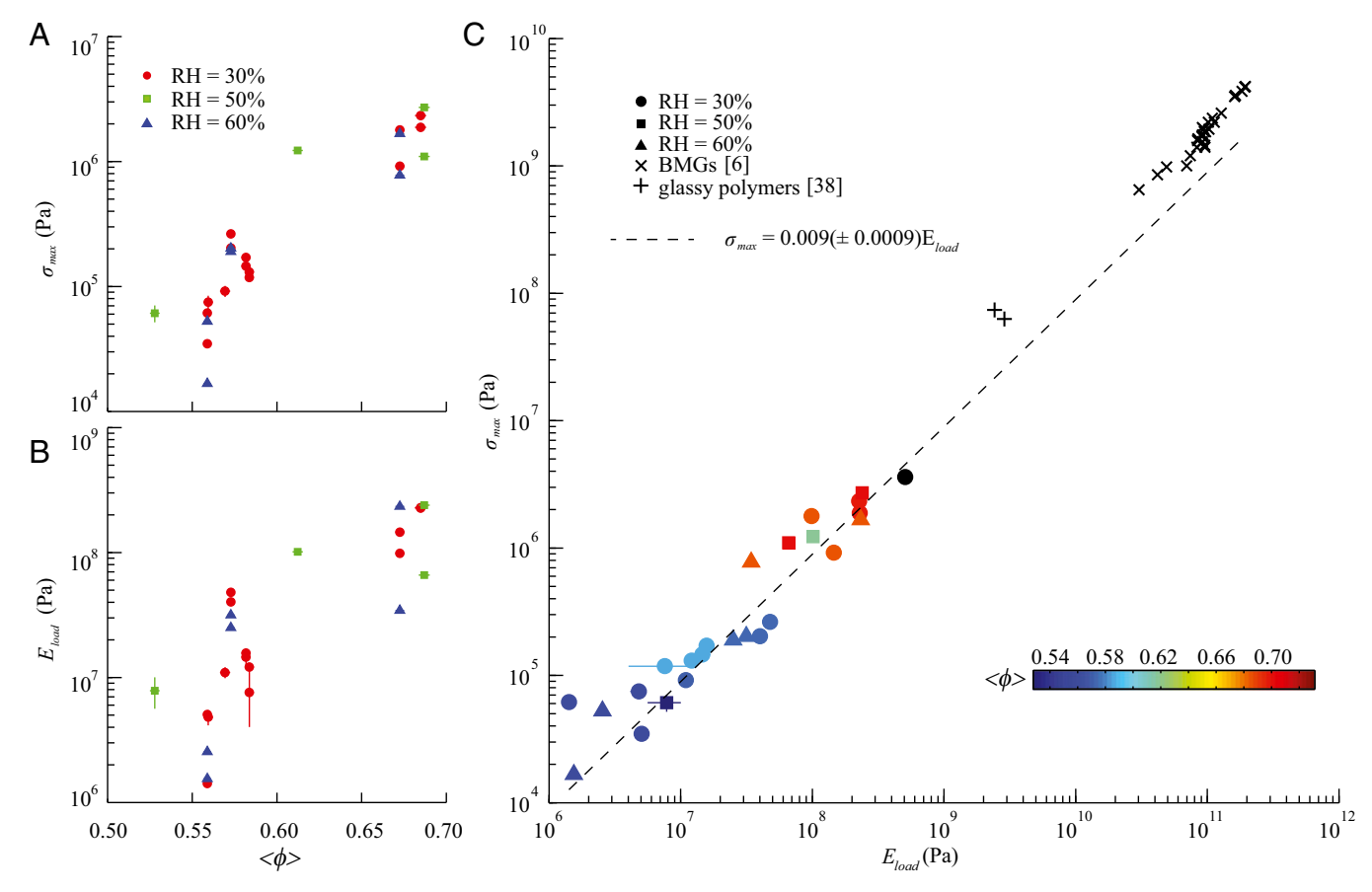


Fig. 2. (A) The normalized maximum transmitted force, σ_{max} vs. $\langle \phi \rangle$, and (B) the normalized stiffness, E_{load} , vs. $\langle \phi \rangle$. See *SI Text* for error analysis. The error is smaller than the data marker for the majority of measurements. (C) The normalized maximum transmitted force, σ_{max} , vs. E_{load} showing a robust correlation that is relatively invariant with $\langle \phi \rangle$ (represented by data marker color; black represents pillars where $\langle \phi \rangle$ measurements were not available). Colloidal micropillar measurements are compared with yield strength and Youngs modulus values for metallic glasses (6) and glassy polymers (38). The dashed line shows the best linear fit to the colloidal data with slope 0.009 \pm 0.0009, representing the critical strain for failure. See *SI Text* for error analysis. The error is smaller than the data marker for the majority of measurements.

Strickland et al. PNAS Early Edition | **3 of 6**

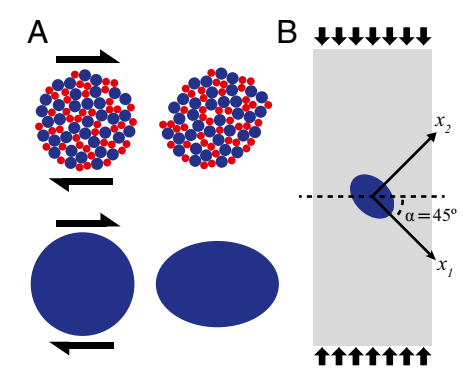


Fig. 3. (*A, Upper*) An idealized cooperative rearrangement induced by an applied shear stress. (*Lower*) A continuum representation of the rearrangement. (*B*) The reference axes defined for the energy analysis. The ellipsoid's major axis, a, lies along x_1 and its minor axis, c, lies along x_2 .

mechanisms of plasticity reminiscent of metallic glasses (e.g., shear banding, pressure-sensitive yield criteria) (28).

To understand the scaling relationship in our relatively athermal colloidal micropillars, we model the fundamental building block of cooperative plastic flow in the framework of Eshelby-like elasticity. Specifically, we consider the change in free energy associated with the introduction of an ellipsoidal inclusion—representing the cooperative shear transformation—in an elastic matrix subjected to an applied far-field stress. This approach is motivated by experiments (15, 17, 29) and simulations (30, 31) on the deformation of amorphous solids that suggest that the fundamental plastic event is a cooperative, shear-induced rearrangement of ~10-100 particles (32), referred to as a shear transformation zone (STZ) (Fig. 3). After operation, in which the STZ evolves from the initial to the deformed state, an elastic strain field is generated in the STZ and the surrounding matrix owing to elastic compatibility. The corresponding change in the Gibbs free energy due to the introduction of an inclusion in a finite elastic matrix subjected to an applied stress has been analyzed using Eshelby's method, where the confined transformation is modeled by allowing for a stress-free unconfined transformation followed by reinsertion into and elastic accommodation by the matrix (33– 35). In addition to the elastic energy of the confined shear transformation, the applied stress field interacts with the stress field generated by the inclusion, resulting in an extra part of the Gibbs free energy (34) (see derivation in SI Text). Taken together, the elastic energy and interaction terms yield a simple expression for the change in the Gibbs free energy associated with the introduction of the inclusion

$$\Delta G = -\frac{1}{2} \int_{\Omega} \sigma_{ij}^{I} \boldsymbol{\epsilon}_{ij}^{T} dV - \int_{\Omega} \sigma_{ij}^{\infty} \boldsymbol{\epsilon}_{ij}^{T} dV$$

$$\Delta G = -\frac{\Omega}{2} \sigma_{ij}^{I} \boldsymbol{\epsilon}_{ij}^{T} - \Omega \sigma_{ij}^{\infty} \boldsymbol{\epsilon}_{ij}^{T}.$$
[1]

Here, σ^I_{ij} is the stress field inside the confined inclusion, ϵ^T_{ij} is the unconfined transformation strain of the inclusion, σ^∞_{ij} is the applied far-field stress, and Ω is the volume of the inclusion. The integrals are readily evaluated because the stress and strain fields inside of an ellipsoidal inclusion are spatially uniform. The stress field inside the inclusion can be written as

$$\sigma_{ij}^{I} = C_{ijkl}(S_{klmn} - \delta_{km}\delta_{ln})\epsilon_{mn}^{T},$$
 [2]

where C_{ijkl} is the stiffness tensor, S_{klmn} is Eshelby's tensor, and δ_{ij} is the Kronecker delta. Eshelby's tensor relates the unconfined transformation strain of the inclusion to the confined strain of the

inclusion (i.e., the strain after being reinserted in the matrix) (33). The shear bands that form in the micropillars are oriented approximately 45° from the pillar axis, which is similar to the orientation of shear bands found in compressed BMGs (bulk metallic glass) (26) and soil pillars (12). Although it is believed that the nature of external loading may bias the orientation of shear bands (toward the pillar axis in compression) (36), we lack the ability to measure shear band orientation to such precision. Therefore, for the energy analysis, we neglect any strong pressure-dependent yielding and assume a triaxial (i.e., each axis is unique in its length, a > b > c) ellipsoidal inclusion with the major axis, a, lying along the direction of maximum shear stress, $\alpha = 45^{\circ}$ (Fig. 3). Following the work of Argon and Shi, we define the transformation strain of the unconfined inclusion as

$$\boldsymbol{\epsilon}_{ij}^T \! = \! \frac{\boldsymbol{\epsilon}_o^T}{3} \! \begin{bmatrix} 1 & 0 & 0 \\ 0 & 1 & 0 \\ 0 & 0 & 1 \end{bmatrix} + \frac{\boldsymbol{\gamma}_o^T}{2} \! \begin{bmatrix} 0 & 1 & 0 \\ 1 & 0 & 0 \\ 0 & 0 & 0 \end{bmatrix},$$

which can be described by the scalar dilatational strain magnitude ϵ_o^T and the the scalar shear strain magnitude γ_o^T . Furthermore, we assume the transformation dilatancy $\beta \equiv \epsilon_o^C/\gamma_o^C \approx 1$ (37). The superscript C denotes the confined transformation strain and may be related to the unconfined transformation strain with superscript T by Eshelby's tensor S_{ijkl} (37). Assuming an isotropic elastic medium, Eq. 2 reduces to

$$\sigma_{ij}^{I} = \frac{2E\epsilon_{o}^{T}}{9(\nu-1)} \begin{bmatrix} 1 & 0 & 0 \\ 0 & 1 & 0 \\ 0 & 0 & 1 \end{bmatrix} + \frac{E\gamma_{o}^{T}(7-5\nu)}{30(\nu^{2}-1)} \begin{bmatrix} 0 & 1 & 0 \\ 1 & 0 & 0 \\ 0 & 0 & 0 \end{bmatrix},$$

where E is Youngs modulus, and ν is Poisson's ratio (39). This expression represents the self-stress of the inclusion, which is completely defined by the material's elastic constants, E and ν , and the transformation strain magnitudes ϵ_o^T and γ_o^T . For uniaxial compression and the reference basis defined in Fig. 3, σ_i^{∞} can be written as

$$\sigma_{ij}^{\infty} = \frac{\sigma}{2} \begin{bmatrix} -1 & 1 & 0 \\ 1 & -1 & 0 \\ 0 & 0 & 0 \end{bmatrix},$$

where $\sigma = F/A_o$ is the applied stress, and compression is negative. Eq. 1 then reduces to

$$\Delta G = \frac{\Omega E}{\nu^2 - 1} \left[\frac{\nu + 1}{9} \left(\frac{\epsilon_o^T}{\beta} \right)^2 + \frac{7 - 5\nu}{60} (\gamma_o^T)^2 \right] + \frac{\Omega \sigma \gamma_o^T}{2} - \frac{\Omega \sigma \epsilon_o^T}{3\beta}. \quad [3]$$

With the assumption that $\beta = 1$, ϵ_o^T can be related to γ_o^T (*SI Text*). We assume that at σ_{max} , $\Delta G = 0$, and on a further increase in the applied stress, the introduction of an inclusion (i.e., operation of a shear transformation) becomes energetically favorable. The relationship between strength and stiffness thus becomes (see *SI Text* for full expression for Θ)

$$\frac{\sigma_{max}}{E} = \gamma_o^T \Theta(\nu, \beta = 1).$$
 [4]

We assume $E=E_{load}$ and values of ν between 0.15 (14) and 0.45 and find a best fit for the data with γ_o^T as the free parameter. Over the range of considered, γ_o^T ranges from 0.026 for $\nu=0.45$ to $\gamma_o^T=0.033$ for $\nu=0.15$; thus, γ_o^T is largely insensitive to ν . Because our system is dissipative, the true elastic modulus is larger than the stiffness measured on loading. Assuming that 50% of the work done on the system during loading is stored as elastic energy (21), the true elastic modulus is underestimated by

a factor of 2 ($2E_{load} = E_{elastic}$; see *SI Text* and Figs. S2 and S3 for load-unload measurements and evidence of quasi-linear loading). This error results in an overestimation of γ_o^T by a factor of 2. Therefore, we take $\gamma_o^T/2$ and γ_o^T as bounds on the magnitude of the characteristic transformation shear strain. Dissipation is likely a result of a combination of frictional sliding at particle contacts and STZ activity. Recent experiments of sheared jammed particles at an interface (12) have shown that below a critical strain of 2%, STZ activity, although present, is minimal. In this confined system, the dramatic increase in STZ operation at the critical strain results in a rapid increase in the loss modulus. In our free-standing pillars, the instability manifests as macroscopic yield and the development of shear bands. Our motivation in setting $\Delta G = 0$ at σ_{max} is to extract a critical strain at which STZs are sufficiently active to lead to shear banding.

The magnitude of γ_o^T found using this analysis of our micropillar data is similar to the values found in simulations of disordered Lennard-Jones particles (39) and experiments of sheared bubble rafts (17) in which displacement fields can be measured directly. Dasgupta et al. compared the nonaffine displacement fields generated by an STZ in a molecular dynamics simulation to the displacement field generated by a general Eshelby transformation strain (39). These authors found good agreement between the fields when using a traceless Eshelby transformation strain with two nonzero eigenvalues and $\gamma_o^T = 0.08$, which agrees well with our value of ~ 0.03 . Argon estimated a shear transformation strain value $\gamma_o^T = 0.125$ based on observations of bubble rafts (32), and Argon and Shi later extracted a range of $\gamma_o^T \approx 0.10 \sim 0.14$ for MGs (37) using a viscoplasticity model. Particle-level measurements of the transformation strain around a rearrangement in a sheared colloidal glass find $\gamma_o^T \approx 0.08 \sim 0.26$ (15). Recent kinetic Monte Carlo (kMC) simulations of MGs that have been successful in capturing shear band formation use a characteristic STZ strain $\gamma_o^T = 0.10$ when determining the free-energy change associated with STZ operation (35, 40, 41). This similiarity in shear transformation kinematics surprisingly extends to other classes of amorphous solids. Simulations of sheared amorphous silicon—a network glass with strongly directional bonding—show $\gamma_o^T \sim 0.015$ (42). The authors of this study note that, although the characteristic size of shear transformations appears to be bonding dependent (~1 nm in metallic glasses, ~3 nm in amorphous silicon, and ~10 nm in glassy polymers) (42), γ_o^T remains similar across systems. Indeed, glassy polymers that are known to develop shear bands on yielding, such as polymethyl methacrylate (PMMA) (43) and PS (44), show shear transformation strains similar to those of MGs ($\gamma_o^T \approx 0.11$ and $\gamma_o^T \approx 0.08$ for PMMA and PS, respectively) (38) (see *SI Text*, Fig. S4, and Table S1 for a table of compiled experimental values of γ_o^T and γ_v for MGs, glassy polymers, and the colloidal micropillars in this work). The robust critical strain appears to break down in glasses that show deformation morphology other than shear banding. For example, the macroscopic critical shear strain in amorphous silica nanowires that exhibit brittle behavior and cleavage fracture is $\gamma_v \approx 0.2$ (45), much larger than the value

found in MGs and glassy polymers. Thus, the cooperative shear mechanism discussed in this work hinges on the intrinsic capacity for plastic flow that precedes final fracture.

This simple model does not capture the complex dynamical interaction of activated and nucleating STZs that determine the ultimate deformation morphology, which likely governs the extent of plastic deformation and the spatio-temporal evolution from individual STZ operation to macroscopic shear localization. However, the robustness of the correlation between σ_{max} and E_{load} for a wide range of structural configurations brought about by mechanical annealing suggests that incipient operation of STZs and macroscopic plastic flow along shear planes occur nearly simultaneously. In other words, the transition from the quasi-elastic to plastic regimes is sharp with respect to stress. This can be inferred as a signature of a system driven in the athermal limit with a relatively narrow distribution of barrier energies defining the fundamental unit of plastic deformation. In contrast to thermal systems, such as metallic glasses, maneuvering within the complex potential energy landscape of our athermal colloidal systems is not aided by thermal activation. We assert that our system is athermal by considering the nondimensional parameter $\frac{k_BT}{\epsilon}$, where k_B is Boltzmann's constant, T is the temperature, and ϵ is a measure of the interaction energy between particles assuming Hertzian contact. This parameter is a measure of the thermal energy relative to the elastic energy stored in the particles and vanishes in the athermal limit. For our system, $\frac{k_BT}{\epsilon} \sim 1 \times 10^{-14}$, much less than the value found in other systems treated as athermal (46). The significance of rate effects that could arise from capillary bridge formation is quantified in the parameter $\dot{\gamma}\tau$, where $\dot{\gamma}$ is the strain rate and τ is the timescale associated with the nucleation of water capillaries. Assuming a capillary nucleation timescale similar to that measured on silicon surfaces (47), $\dot{\gamma}\tau \sim 1 \times 10^{-11}$, indicating that nucleation events occur at timescales much smaller than the timescale associated with the imposed strain. With thermal fluctuations absent, the applied stress alone surmounts the local energy maxima, ultimately driving the cooperative events. In turn, the compatibility constraint of the elastic matrix on shear transformation (cooperative rearrangement of a collection of particles with a characteristic shear strain γ_o^T) provides the longrange interaction to drive localized failure. Taken as a whole, the similarities in macroscopic yielding strain, characteristic STZ strain, and shear band morphology between our colloidal packings and metallic glasses, despite the dissipative nature of our particle-particle interactions, lend support to the notion of a universal cooperative plastic event unique to amorphous solids with the capacity for plastic flow.

ACKNOWLEDGMENTS. We thank the Penn Nanoscale Characterization Facility for technical support and D. J. Magagnoss for technical assistance and insightful discussions. We also thank A. Liu for critical reading of our manuscript and insightful comments. We gratefully acknowledge financial support from the National Science Foundation through University of Pennsylvania Materials Science Research and Engineering Center DMR-1120901.

- Frenkel J (1926) Zur Theorie der Elastizittsgrenze und der Festigkeit kristallinischer Krper. Z Phys 37(7-8):572-609.
- Hall EO (1951) The deformation and ageing of mild steel: III discussion of results. Proc Phys Soc B 64(9):747–753.
- 3. Petch N (1953) The cleavage strength of polycrystals. J Iron Steel Inst 174(1953):25–28.
- Taylor GI (1934) The mechanism of plastic deformation of crystals. Part I. Theoretical. Proc R Soc Lond A Math Phys Sci 145(855):362–387.
- Inoue A, Takeuchi A (2011) Recent development and application products of bulk glassy alloys. Acta Mater 59(6):2243–2267.
- Johnson WL, Samwer K (2005) A universal criterion for plastic yielding of metallic glasses with a (T/Tg)2/3 temperature dependence. Phys Rev Lett 95(19):195501.
- glasses with a (T/Tg)2/3 temperature dependence. *Phys Rev Lett* 95(19):195501.

 7. Cheng Y, Ma E (2011) Intrinsic shear strength of metallic glass. *Acta Mater* 59(4):1800–1807.
- Wu F, Zhang Z, Mao S, Peker A, Eckert J (2007) Effect of annealing on the mechanical properties and fracture mechanisms of a Zr56.2Ti13.8Nb5.0Cu6.9Ni5.6Be12.5 bulkmetallic-glass composite. Phys Rev B 75(13):134201.
- Scudino S, Jerliu B, Surreddi K, Kühn U, Eckert J (2011) Effect of cold rolling on compressive and tensile mechanical properties of Zr52.5Ti5Cu18Ni14.5Al10 bulk metallic glass. J Alloys Compd 509(Suppl 1):S128–S130.
- Magagnosc D, et al. (2014) Effect of ion irradiation on tensile ductility, strength and fictive temperature in metallic glass nanowires. Acta Mater 74:165–182.
- Xiao Q, Huang L, Shi Y (2013) Suppression of shear banding in amorphous ZrCuAl nanopillars by irradiation. J Appl Phys 113(8):083514.
- Desrues J, Chambon R (2002) Shear band analysis and shear moduli calibration. Int J Solids Struct 39(13-14):3757–3776.
- Chikkadi V, Wegdam G, Bonn D, Nienhuis B, Schall P (2011) Long-range strain correlations in sheared colloidal glasses. *Phys Rev Lett* 107(19):198303.
- Zhang L, et al. (2013) Using shape anisotropy to toughen disordered nanoparticle assemblies. ACS Nano 7(9):8043–8050.
- Schall P, Weitz DA, Spaepen F (2007) Structural rearrangements that govern flow in colloidal glasses. Science 318(5858):1895–1899.

- 16. Chikkadi V, Schall P (2012) Nonaffine measures of particle displacements in sheared colloidal glasses. Physical Review E 85(3):031402.
- 17. Argon A, Kuo H (1979) Plastic flow in a disordered bubble raft (an analog of a metallic glass). Mater Sci Eng 39(1):101-109.
- 18. Demetriou MD, et al. (2006) Cooperative shear model for the rheology of glassforming metallic liquids. Phys Rev Lett 97(6):65502.
- 19. Falk ML, Langer JS (1998) Dynamics of viscoplastic deformation in amorphous solids. Phys Rev E Stat Phys Plasmas Fluids Relat Interdiscip Topics 57(6):7192–7205.
- 20. Langer JS (2006) Shear-transformation-zone theory of deformation in metallic glasses. Scr Mater 54(3):375-379.
- 21. Strickland DJ, et al. (2014) Synthesis and mechanical response of disordered colloidal micropillars. Phys Chem Chem Phys 16(22):10274-10285.
- 22. Farr RS, Groot RD (2009) Close packing density of polydisperse hard spheres. J Chem Phys 131(24):244104.
- 23. Shapiro AP, Probstein RF (1992) Random packings of spheres and fluidity limits of monodisperse and bidisperse suspensions. Phys Rev Lett 68(9):1422-1425.
- 24. Schuh C, Hufnagel T, Ramamurty U (2007) Mechanical behavior of amorphous alloys. Acta Mater 55(12):4067-4109.
- 25. Chen M (2008) Mechanical behavior of metallic glasses: Microscopic understanding of strength and ductility. Ann Rev Mater Res 38:445-469.
- 26. Greer A, Cheng Y, Ma E (2013) Shear bands in metallic glasses. Mater Sci Eng Rep 74(4):71-132.
- 27. Rupert TJ (2014) Solid solution strengthening and softening due to collective nanocrystalline deformation physics. Scr Mater 81:44-47.
- 28. Trelewicz JR. Schuh CA (2007) The HallPetch breakdown in nanocrystalline metals: A crossover to glass-like deformation. Acta Mater 55(17):5948-5958.
- 29. Keim NC, Arratia PE (2013) Yielding and microstructure in a 2D jammed material under shear deformation. Soft Matter 9(27):6222.
- 30. Deng D, Argon AS, Yip S (1989) Simulation of plastic deformation in a two-dimensional atomic glass by molecular dynamics IV. Philos Trans R Soc Lond A 329(1608):613-640.
- 31. Srolovitz D, Maeda K, Vitek V, Egami T (1981) Structural defects in amorphous solids Statistical analysis of a computer model. Philos Mag A 44(4):847-866.

- 32. Argon A (1979) Plastic deformation in metallic glasses. Acta Metall 27(1):47-58.
- 33. Eshelby JD (1957) The determination of the elastic field of an ellipsoidal inclusion, and related problems. Proc R Soc Math Phys Eng Sci 241(1226):376–396.
- 34. Mura T (1987) Micromechanics of Defects in Solids (Springer, Berlin), Vol 3.
- 35. Homer ER (2014) Examining the initial stages of shear localization in amorphous metals. Acta Mater 63:44-53.
- 36. Gao YF, Wang L, Bei H, Nieh TG (2011) On the shear-band direction in metallic glasses. Acta Mater 59(10):4159-4167.
- 37. Argon A, Shi L (1983) Development of visco-plastic deformation in metallic glasses. Acta Metall 31(4):499-507.
- 38. Kozey VV, Kumar S (1994) Compression behavior of materials: Part I. Glassy polymers. J Mater Res 9(10):2717-2726.
- 39. Dasgupta R, Gendelman O, Mishra P, Procaccia I, Shor CABZ (2013) Shear localization in three-dimensional amorphous solids. Phys Rev E Stat Nonlin Soft Matter Phys 88(3):32401.
- 40. Homer ER, Schuh CA (2009) Mesoscale modeling of amorphous metals by shear transformation zone dynamics. Acta Mater 57(9):2823-2833.
- 41. Homer ER, Rodney D, Schuh CA (2010) Kinetic Monte Carlo study of activated states and correlated shear-transformation-zone activity during the deformation of an amorphous metal. Phys Rev B 81(6):064204.
- 42. Argon AS, Demkowicz MJ (2006) Atomistic simulation and analysis of plasticity in amorphous silicon. Philos Mag 86(25-26):4153-4172.
- 43. Bowden PB, Raha S (1970) The formation of micro shear bands in polystyrene and polymethylmethacrylate. Philos Mag 22(177):463-482.
- 44. Argon AS, Andrews RD, Godrick JA, Whitney W (1968) Plastic deformation bands in glassy polystyrene. J Appl Phys 39(3):1899-1906.
- 45. Brambilla G, Payne DN (2009) The ultimate strength of glass silica nanowires. Nano Lett 9:831-835.
- 46. Basu A, et al. (2014) Rheology of soft colloids across the onset of rigidity: Scaling behavior, thermal, and non-thermal responses. Soft Matter 10(17):3027-3035.
- 47. Greiner C, Felts JR, Dai Z, King WP, Carpick RW (2010) Local nanoscale heating modulates single-asperity friction. Nano Lett 10(11):4640-4645.

Supporting Information

Strickland et al. 10.1073/pnas.1413900111

SI Text

Error and Uncertainty Analysis. The uncertainties in measured quantities, δ , are

transmitted force $\delta_F = \begin{cases} 5 \times 10^{-3} & N & 1000 & g-F \text{ transducer} \\ 5 \times 10^{-4} & N & 100 & g-F \text{ transducer} \\ 5 \times 10^{-5} & N & 10 & g-F \text{ transducer} \end{cases}$

specimen diameter $\delta_D = 2 \, \mu \text{m}$,

specimen cross-sectional area $\delta_{A_0} = \sqrt{(\delta_D)^2 (\pi D)^2}$,

specimen length $\delta_{l_0} = 2 \, \mu \text{m}$,

specimen change in length $\delta_{\Delta l} = 10 \times 10^{-4} \times l_o$,

unfilled capillary mass $\delta_{m_{unfilled}} = 2 \, \mu g$,

filled capillary mass $\delta_{m_{filled}} = 2 \mu g$,

micropillar length in capillary $\delta_L = 10 \, \mu \text{m}$.

We assume an uncorrelated propagation of error. The uncertainties in the reported quantities $\langle \phi \rangle$, σ_{max} , and E_{load} are given by

$$\langle \phi \rangle = \frac{\left(m_{filled} - m_{empty} \right) / \rho_{PS}}{\pi (D/2)^2 L},$$

with $\epsilon_{total} = \epsilon_{elastic} + \epsilon_{plastic}$. By construction, $\eta = \frac{\epsilon_{elastic}}{\epsilon_{total}}$, so rearranging yields

$$E_{load} = \eta E_{unload}$$
.

Assuming $\eta = 50\%$, we underestimate the elastic component of stiffness (E_{unload}) by a factor of 2, i.e., $2E_{load} = E_{unload}$. Because the transformation strain magnitude, ϵ^* , is inversely proportional to $E(\gamma_0^T \propto 1/E; \text{ Eq. 4})$, we overestimate the transformation strain by a factor of 2 by using E_{load} in the energy analysis. Therefore, our reported value for γ_o^T should be considered an upper bound.

In previous experiments, we quantified the dissipation in a specimen when compressed to small strains as a function of RH. Briefly, we found a strong dependence of η on RH with a significant decrease in η —equivalently, an increase in dissipation—for RH above ~40%. An example of an experimental compression cycle at RH = 50% is shown in Fig. S3.

Gibbs Free Energy of an Inclusion in an Elastic Matrix. For completeness, we reproduce the derivation by Mura (2) of the change in the Gibbs free energy, G, of an inclusion in an elastic matrix with an applied traction. Define

$$\delta_{\langle \phi \rangle} = \sqrt{ \left(\delta_{m_{\mathit{filled}}} \right)^2 \left(\frac{1}{\rho_{\mathit{ps}} A_o L} \right)^2 + \left(\delta_{m_{\mathit{empty}}} \right)^2 \left(\frac{-1}{\rho_{\mathit{ps}} A_o L} \right)^2 + \left(\delta_{A_o} \right)^2 \left(\frac{m_{\mathit{empty}} - m_{\mathit{filled}}}{\rho_{\mathit{ps}} A_o^2 L} \right)^2 + \left(\delta_L \right)^2 \left(\frac{m_{\mathit{empty}} - m_{\mathit{filled}}}{\rho_{\mathit{ps}} A_o L^2} \right)^2},$$

$$\sigma_{max} = \frac{F}{A_o}$$

$$\delta_{\sigma_{max}} = \sqrt{\left(\delta_{F_{max}}\right)^2 \left(\frac{1}{A_0}\right)^2 + \left(\delta_{A_o}\right)^2 \left(\frac{-F_{max}}{A_0^2}\right)^2},$$

$$E_{load} \propto \frac{Fl_o}{A_o \Delta l}$$

$$\delta E_{load} = \sqrt{ \left(\delta_F \right)^2 \! \left(\! \frac{l_o}{A_o \Delta l} \! \right)^2 + \left(\delta_{l_o} \right)^2 \! \left(\! \frac{F}{A_o \Delta l} \! \right)^2 + \left(\delta_{A_o} \right)^2 \! \left(\! \frac{-Fl_o}{A_o^2 \Delta l} \! \right)^2 + \left(\delta_{\Delta l} \right)^2 \! \left(\! \frac{-Fl_o}{A_o \Delta l^2} \! \right)^2 } \, . \label{eq:delta_E_load}$$

For the linear fit of $\sigma_{max} = \beta E_{load}$, we report the 95% CI for the regression analysis.

Effects of Dissipation in Stiffness Determination. Prior work (1) has shown that the micropillars are quite dissipative even at small strains. We define an efficiency, η , which is the ratio of work done by the pillar on loading to the work done on the pillar during loading

$$\eta = \frac{W_{unload}}{W_{load}} = \frac{E_{unload} \epsilon_{elastic}^2}{E_{load} \epsilon_{total}^2},$$

$$\epsilon_{ij} = \frac{1}{2} \left(\frac{\partial u_i}{\partial x_j} + \frac{\partial u_j}{\partial x_i} \right) \equiv \text{total strain},$$

 $\epsilon_{ii}^* \equiv$ eigenstrain or transformation strain,

 $e_{ii} \equiv \text{elastic strain},$

$$\sigma_{ii} = C_{iikl}e_{kl} \equiv \text{stress}.$$

The elastic strain energy of a body subjected to an applied traction σ_{ii}^{∞} and an internal stress due to an inclusion σ_{ij} is given by

$$W^* = \frac{1}{2} \int_{V} \left(\sigma_{ij}^{\infty} + \sigma_{ij} \right) \left(\epsilon_{ij}^{\infty} + \epsilon_{ij} - \epsilon_{ij}^* \right) dV \quad \text{with} \quad \sigma_{ij}^{\infty} = C_{ijkl} \epsilon_{ij}^{\infty}.$$

Equilibrium ensures that $\sigma_{ij,j} = 0$ and $\sigma_{ij}n_j = 0$ at the surface S. Integration by parts gives

$$\int_{V} \sigma_{ij} \left(\epsilon_{ij}^{\infty} + \epsilon_{ij} \right) dV = \int_{V} \sigma_{ij} \left(u_{i,j}^{\infty} + u_{i,j} \right) dV,$$

$$=\sigma_{ij}\left(u_{ij}^{\infty}+u_{ij}\right)\Big|_{V=S}-\int\limits_{V}\sigma_{ij,j}\left(u_{ij}^{\infty}+u_{ij}\right)dV=0.$$

Similarly, $\sigma_{ij,j}^{\infty} = 0$. Because $\epsilon_{ij}^{\infty} = e_{ij}^{\infty}$ and $e_{ij} = \epsilon_{ij} - \epsilon_{ij}^{*}$ and using the symmetry $C_{ijkl} = C_{klij}$

$$= \int_{V} u_{k,l}^{\infty} \sigma_{kl} dV = u_{kl} \sigma_{kl} \bigg|_{V=S} - \int_{V} u_{kl}^{\infty} \sigma_{kl,l} dV = 0.$$

So

$$W^* = -\frac{1}{2} \int\limits_V \sigma_{ij} \epsilon_{ij}^* dV + \frac{1}{2} \int\limits_V \sigma_{ij}^\infty \epsilon_{ij}^\infty dV.$$

The total potential energy is given by

$$G = W^* - \int_{S} F_i^{\infty} (u_i + u_i^{\infty}) dS,$$

where the second term is the work done at the boundary by the applied traction, and $F_i^{\infty} = \sigma_{ij}^{\infty} n_j$. Without any inclusions ($\epsilon_{ij}^* = 0$), $G = G_o$

$$G_o = \frac{1}{2} \int\limits_{V} \sigma_{ij}^{\infty} \epsilon_{ij}^{\infty} dV - \int\limits_{S} F_i^{\infty} u_{ij}^{\infty} dS.$$

Without any applied tractions ($\sigma_{ii}^{\infty} = 0$), $G = G_1$

$$G_1 = -\frac{1}{2} \int\limits_V \sigma_{ij} \epsilon_{ij}^* dV.$$

The interaction between the strain field generated by the inclusions and the applied traction is

$$\Delta G = G - G_o - G_1 = -\int_{S} \sigma_{ij}^{\infty} u_i n_j dS = -\int_{V} \sigma_{ij}^{\infty} u_{i,j} dV$$
$$= -\int_{V} \sigma_{ij}^{\infty} \left(u_{i,j} - \epsilon_{ij}^* \right) dV - \int_{V} \sigma_{ij}^{\infty} \epsilon_{ij}^* dV = -\int_{V} \sigma_{ij}^{\infty} \epsilon_{ij}^* dV.$$

by Gauss's theorem and the fact that $\int \sigma_{ij}^{\infty}(u_{i,j} - \epsilon_{ij}^*)dV = 0$ (see above). Therefore, with spatially homogeneous stress and strain fields

$$\Delta G = -\int_{V} \sigma_{ij}^{\infty} \boldsymbol{\epsilon}_{ij}^{*} dV = -\sigma_{ij}^{\infty} \boldsymbol{\epsilon}_{ij}^{*}.$$

For the case where the body is under an applied traction and inclusions are introduced, the change in free energy is given by

$$\Delta \overline{G} = G - G_o = \Delta G + G_1 = -\frac{1}{2} \sigma_{ij} \epsilon_{ij}^* - \sigma_{ij}^\infty \epsilon_{ij}^*,$$

which is Eq. 1.

Derivation of the Stress Field for a Prescribed Transformation Strain. The tensorial infinitesimal strain, ϵ_{ii} , is given by

$$\epsilon_{ij} = \frac{1}{2} \begin{pmatrix} \frac{\partial u_i}{\partial x_j} + \frac{\partial u_j}{\partial x_i} \end{pmatrix} = \begin{pmatrix} \epsilon_{11} & \epsilon_{12} & \epsilon_{13} \\ \epsilon_{12} & \epsilon_{22} & \epsilon_{23} \\ \epsilon_{13} & \epsilon_{23} & \epsilon_{33} \end{pmatrix} = \begin{pmatrix} \epsilon_{11} & \frac{\gamma_{12}}{2} & \frac{\gamma_{13}}{2} \\ \frac{\gamma_{12}}{2} & \epsilon_{22} & \frac{\gamma_{23}}{2} \\ \frac{\gamma_{13}}{2} & \frac{\gamma_{23}}{2} & \epsilon_{33} \end{pmatrix}.$$

Define the stiffness tensor, C_{ijkl} , for an isotropic homogeneous solid as

$$C_{ijkl} = \frac{E\nu}{(1+\nu)(1-2\nu)} \delta_{ij} \delta_{kl} + \frac{E}{2(1+\nu)} \left(\delta_{ik} \delta_{jl} + \delta_{il} \delta_{jk} \right),$$

and the constitutive relation

$$\sigma_{ii} = C_{iikl} \epsilon_{kl}$$

where ϵ_{kl} is now the elastic component of the strain. Argon and Shi (3) use Eshelby's tensor for a spherical inclusion, given by

$$S_{ijkl} = \frac{5\nu - 1}{15(1 - \nu)} \delta_{ij} \delta_{kl} + \frac{4 - 5\nu}{15(1 - \nu)} \left(\delta_{ik} \delta_{jl} + \delta_{il} \delta_{jk} \right).$$

To relate the confined strain, ϵ_{ij}^C , to the transformation strain, ϵ_{ij}^T , of the inclusion

$$\epsilon_{ii}^c = S_{iikl} \epsilon_{kl}^T$$
.

The authors assume two components of ϵ_{kl}^T

$$\boldsymbol{\epsilon}_{kl}^T \! = \! \frac{\boldsymbol{\epsilon}_o^T}{3} \begin{pmatrix} 1 & 0 & 0 \\ 0 & 1 & 0 \\ 0 & 0 & 1 \end{pmatrix} + \frac{\gamma_o^T}{2} \begin{pmatrix} 0 & 1 & 0 \\ 1 & 0 & 0 \\ 0 & 0 & 0 \end{pmatrix},$$

where the first term accounts for dilatation and the second for a pure shear. The stress inside the inclusion, σ_{ii}^L , is given by

$$\sigma_{ii}^{I} = C_{ijkl} (S_{klmn} \epsilon_{mn}^{T} - \epsilon_{kl}^{T}).$$

The elastic energy in both the inclusion and matrix is given as

$$E_{elastic} = -\frac{1}{2} \int_{\Omega_{\rm f}} \sigma_{ij}^I \epsilon_{ij}^T dV.$$

For the case of a spherical inclusion, in which σ^I_{ij} and ϵ^T_{ij} are constants, this expression becomes

$$E_{elastic} = -\frac{1}{2} \sigma_{ij}^{I} \epsilon_{ij}^{T} \Omega_{f}.$$

Considering only the dilatational component of ϵ_{kl}^T and using the relationship $E = 2\mu(1 + \nu)$

$$\sigma_{ij}^{I} = \frac{2E\epsilon_{o}^{T}}{9(\nu - 1)} \begin{pmatrix} 1 & 0 & 0\\ 0 & 1 & 0\\ 0 & 0 & 1 \end{pmatrix} \quad \text{and} \quad E_{elastic} = \frac{E}{9(1 - \nu)} (\epsilon_{o}^{T})^{2}$$
$$= \frac{2\mu(1 + \nu)}{9(1 - \nu)} (\epsilon_{o}^{T})^{2},$$

which is the same as the second term of equation 7 in ref. 3. Now, considering only the shear component of ϵ_{kl}^T yields

$$\sigma_{ij}^{I} = \frac{E\gamma_o^T (7 - 5\nu)}{30(\nu^2 - 1)} \begin{pmatrix} 0 & 1 & 0\\ 1 & 0 & 0\\ 0 & 0 & 0 \end{pmatrix} \text{ and }$$

$$E_{elastic} = \frac{E(7 - 5\nu)}{60(1 - \nu^2)} (\gamma_o^T)^2 = \frac{\mu(7 - 5\nu)}{30(1 - \nu)} (\epsilon_o^T)^2,$$

which is the same as the first term of equation 7 in ref. 3. In the presence of an applied far-field stress, the change in Gibb's free energy becomes (see previous section)

$$\Delta G = -\frac{1}{2} \sigma_{ij}^I \epsilon_{ij}^T \Omega_f - \sigma_{ij}^\infty \epsilon_{ij} \Omega_f.$$

For uniaxial compression and our assumed orientation of the inclusion, the applied stress is

$$\sigma_{ij} = \frac{\sigma}{2} \begin{pmatrix} -1 & 1 & 0 \\ 1 & -1 & 0 \\ 0 & 0 & 0 \end{pmatrix}.$$

Therefore, the change in free energy is

$$\Delta G = \frac{E}{\nu^2 - 1} \left[\frac{\nu + 1}{9} \left(\epsilon_o^T \right)^2 + \frac{7 - 5\nu}{60} \left(\gamma_o^T \right)^2 \right] - \frac{\sigma \left(2\epsilon_o^T - 3\gamma_o^T \right)}{6}.$$

Argon and Shi define the transformation dilatancy as

$$\beta = \frac{\epsilon_o^c}{\gamma_o^c} = \frac{45(1-\nu)^2 \epsilon_o^T}{2(1+\nu)(4-5\nu)\gamma_o^T}.$$

- Strickland DJ, et al. (2014) Synthesis and mechanical response of disordered colloidal micropillars. Phys Chem Chem Phys 16(22):10274–10285.
- 2. Mura T (1987) Micromechanics of Defects in Solids (Springer, Berlin), Vol 3.

From measurements on an amorphous bubble raft, the authors estimate $\beta \approx 1$ (3). Therefore

$$\epsilon_o^T = \gamma_o^T \frac{2(1+\nu)(4-5\nu)}{45(1-\nu)^2},$$

with this relationship

$$\Delta G = \frac{\Omega E}{\nu^2 - 1} \left\{ \frac{\nu + 1}{9} \left[\frac{2(1 + \nu)(4 - 5\nu)}{45(1 - \nu)^2} \gamma_o^T \right]^2 + \frac{7 - 5\nu}{60} (\gamma_o^T)^2 \right\} + \frac{\Omega \sigma \gamma_o^T}{2} - \frac{\Omega \sigma \gamma_o^T}{3} \frac{2(1 + \nu)(4 - 5\nu)}{45(1 - \nu)^2}.$$

Setting $\Delta G = 0$ and rearranging yields

$$\begin{split} \frac{\sigma}{E} &= \frac{\gamma_o^T \left[5,675\nu^5 - 33,365\nu^4 + 70,934\nu^3 - 74,578\nu^2 + 39,967\nu - 8,761 \right]}{270(\nu - 1)^3 (155\nu^3 - 111\nu^2 - 147\nu + 119)} \\ &\equiv \gamma_o^T \theta(\nu). \end{split}$$

 Argon AS, Shi L (1983) Development of visco-plastic deformation in metallic glasses. Acta Metall 31(4):499–507.

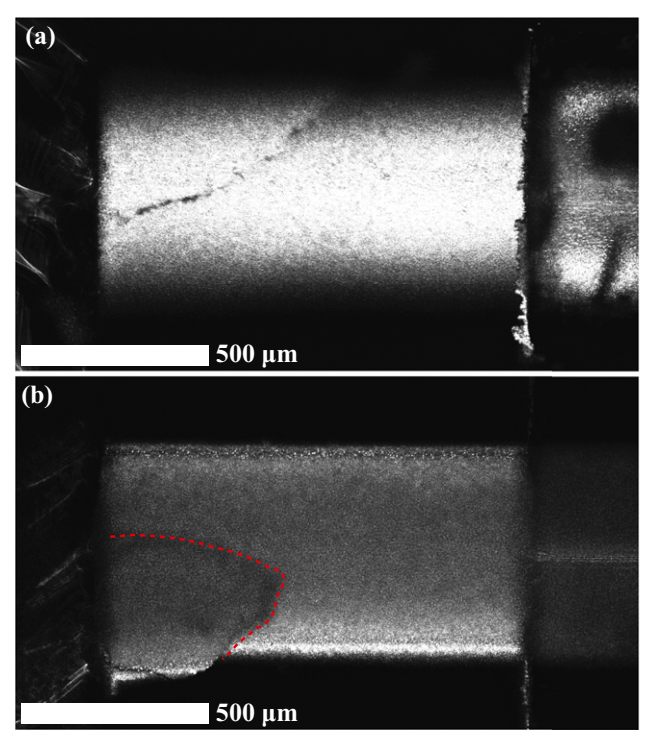


Fig. S1. Laser-scanning confocal micrographs of deformed micropillar specimens. (A) A specimen with $\phi = 0.559$ compressed at RH = 60%. Failure results from the development of a shear band that propagates from the specimen/punch interface to the specimen surface. (B) A specimen with $\phi = 0.687$ compressed at RH = 50%. The darker region outlined by the dashed red line has been sheared out of plane.

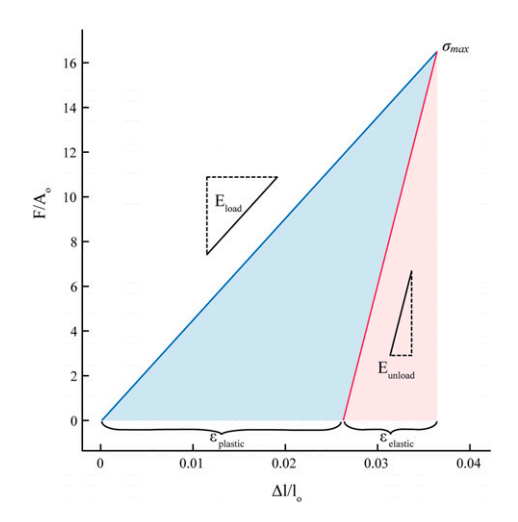


Fig. S2. Idealized compressive response showing loading and unloading moduli.

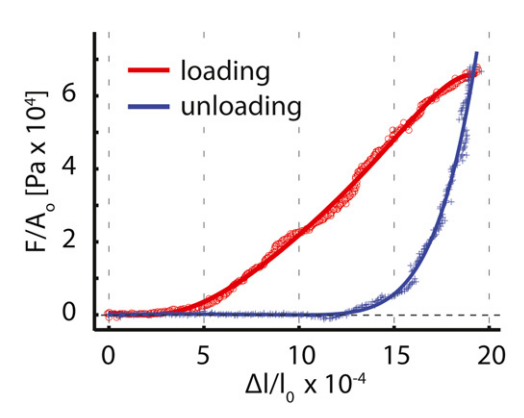


Fig. S3. Experimental compressive response of a colloidal micropillar at 50% RH. The stiffness on unloading is larger than the measured stiffness on loading.

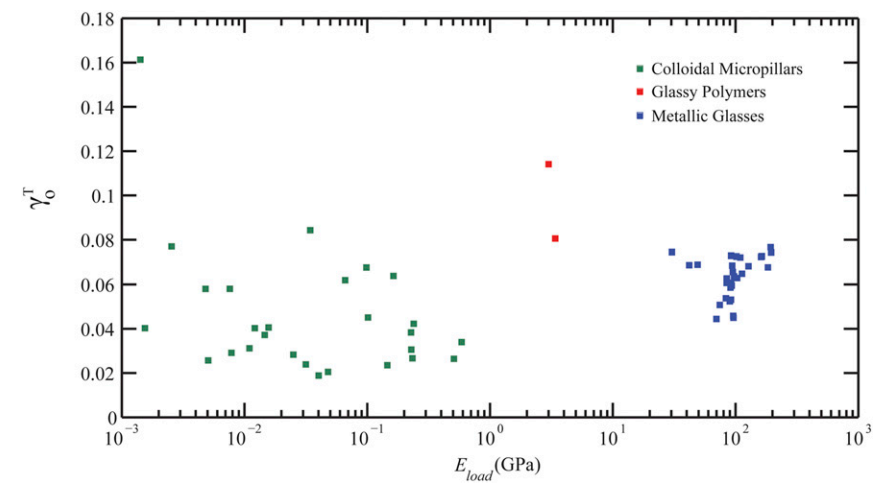


Fig. S4. A comparison of the shear component of the transformation strain, γ_0^T , for colloidal micropillars, glassy polymers, and metallic glasses (see Table S1 for values and references). Atlhough the elastic moduli of the materials span five orders of magnitude, the kinematics of the proposed plastic event remain remarkably similar.

Table 51. Comparison of macroscopic critical and transformation strains in amorphous solids

Symbol	symbol Definition . MGs (1, 2) . Glassy p	MGs (1,	1, 2)	Glassy	Glassy polymers (3)	Confin	Confined colloidal glass (4)	Colloidal mic	Colloidal micropillars $[0.15 < \nu < 0.45]$
7,	Macroscopic critical shear strain	Definition	$\eta/\lambda_2 =$	Definition	$= \frac{\sigma_{\max}(1+\nu)}{E}$	Definition	Definition Macroscopic shear strain Definition at formation of the first rearrangement	Definition	$= \frac{\sigma_{max}(1+\nu)}{E_{load}}$
		Range Mean	= 0.020 - 0.030 Range = 0.026 Mean	0 Range Mean	= 0.031 - 0.044 $= 0.038$	Range Mean	= 0.012 NA	Range Mean	= 0.006 - 0.063 $= 0.016$
$\epsilon_{\mathcal{Y}}$	Macroscopic critical axial strain	SD Definition Range	$= 0.003 = \sigma_y / E = 0.014 - 0.022$	SD Definition 2 Range	$= 0.009 = \sigma_y / E = 0.024 - 0.033$	SD Definition Range	4 4 4 7 7 7	SD Definition Range	$= 0.010 = \sigma_{max} / E_{load} = 0.005 - 0.043$
١		Mean SD	= 0.0	Mean SD	=0.028 =0.007	Mean SD	- V V V V V	Mean SD	= 0.012 = 0.008
7,0	Shear component of eigenstrain or unconfined transformation strain	Definition Visco-plastic model in ref.	Eq. 4 ref. 1	Definition	Еq. 4	Definition	Average particle-level shear strain around a rearrangement	Definition	Eq. 4
		Range $= 0.11 - 0.14$ Mean $= 0.12$ SD $= 0.012$	1 = 0.044 – 0.077 Range = 0.063 Mean = 0.009 SD	7 Range Mean SD	=0.081-0.114 Range =0.097 Mean =0.023 SD	Range Mean SD	≈ 0.08 – 0.26 NA NA	Range Mean SD	= 0.014 - 0.161 $= 0.041$ $= 0.026$

NA, not applicable.

Argon AS, Shi L (1983) Development of visco-plastic deformation in metallic glasses. Acta Metall 31(4):499–507.
 Johnson WU, Samwer K (2005) A universal criterion for plastic yielding of metallic glasses with a (T/T g) 2/3 temperature dependence. Phys Rev Lett 95(19):195501.
 Kozey VV, Kumar S (1994) Compression behavior of materials: Part I. Glassy polymers. J Mater Res 9(10):2717–2726.
 Schall P, Weitz DA, Spaepen F (2007) Structural rearrangements that govern flow in colloidal glasses. Science 318(5858):1895–1899.